Resonant control of spins in the quasi-one-dimensional channel by interplay of confinement and Zeeman splitting

D. H. Berman, M. Khodas, and M. E. Flatté

Citation: AIP Conference Proceedings **1619**, 33 (2014); doi: 10.1063/1.4899215
View online: http://dx.doi.org/10.1063/1.4899215
View Table of Contents: http://scitation.aip.org/content/aip/proceeding/aipcp/1619?ver=pdfcov
Published by the AIP Publishing

Resonant control of spins in the quasi-one-dimensional channel by interplay of confinement and Zeeman splitting

D. H. Berman, M. Khodas and M. E. Flatté

Department of Physics and Astronomy, University of Iowa, Iowa City, Iowa 52242, USA

Abstract. We study the spin transport in a quasi-one-dimensional channel defined in a two-dimensional electron gas. The combined action of geometrical confinement and the spin precession is analyzed. We demonstrate that for certain orientations of the in-plane magnetic field and for specific range of its magnitude the spin polarization exhibits a strong decrease referred to as ballistic spin resonance (BSR). The phenomenon is due to the commensuration of the Zeeman and inter-subband energy splitting. We show that the BSR requires a finite spin-orbit (SO) interaction although the condition for the BSR onset is independent on SO coupling.

Keywords: Spintronics, quasi-one-dimensional transport
PACS: 72.25.-b, 72.25.Hg, 73.23.Ad

THE BACKGROUND AND MOTIVATION

Controlling of spin relaxation in low-dimensional structures is one of the most promising directions in the field of spin based electronics, i.e. spintronics [1, 2, 3, 4, 5, 6]. The geometrical confinement is known to suppress the spin relaxation in spin-orbit (SO) coupled systems [7, 8, 9, 10, 11, 12, 13]. This has been demonstrated directly in InGaAs submicron wires by means of time-resolved Faraday rotation in a pump-probe set up, [14]. The SO interaction provides an effective Zeeman field determined by the orbital momentum. The impurity scattering randomizes the electron momentum and hence the direction of the effective Zeeman field. Therefore, the spin precession acquires the random character and leads to the spin relaxation. The spatial confinement counteracts the randomizing effect of the impurity scattering and therefore suppresses the spin relaxation. Similarly, the in-plane magnetic field adds a constant component to the SO induced effective field, and suppresses the spin relaxation [15, 16].

Surprisingly, however the combination of geometrical confinement and the in-plane Zeeman field may under certain conditions cause enhancement of the spin relaxation. Such is the case in the Ballistic Spin Resonance (BSR) experiment by Frolov *et. al.*, [17, 18] in the quasi-one-dimensional channel hosting a few tens of conduction channels, Fig. 1. In this experiment the lithographically defined channel is contacted by three identical quantum point contacts tuned to e^2/h conductance in the presence of the spin splitting magnetic field. The spin-polarized current is driven between the two contacts and the induced non-local voltage is detected at the third quantum point contact along the channel in the region with zero electrical current. In the absence of heat transfer the non-local signal is induced due to the imbalance in spin polarization.

The main observation for the case of the in-plane magnetic field is the suppression of the non-local voltage when the field is directed perpendicular to the channel, Fig. 1. No such effect is observed when the magnetic field is directed along the channel. Here we construct the theory of BSR following [19] and show how it accounts for most of the observed features.

THEORY OF BSR FOLLOWING REF. [19]

The model

The Hamiltonian describing the motion and spin dynamics of electrons in the channel takes the form,

$$H = \frac{p_x^2 + p_z^2}{2m} + V_c(z) - \frac{1}{2} E_Z \sigma_z + H_{SO}\,. \tag{1}$$

The Fourth Conference on Nuclei and Mesoscopic Physics 2014
AIP Conf. Proc. 1619, 33-39 (2014); doi: 10.1063/1.4899215

Here $V_c(z)$ is the lateral confinement potential, E_Z is the Zeeman splitting, and

$$H_{SO} = \alpha_- p_z \sigma_x + \alpha_+ p_x \sigma_z \tag{2}$$

is the SO interaction term with $\alpha_{+,(-)}$ equal to the sum (difference) of the Rashba [20, 21] and Dresselhaus [22] coefficients. The term with α_+ is proportional to σ_z. It therefore does not couple subbands with opposite spin polarization along $\hat{z}$. Hence we neglect this term, $\alpha_+ = 0$ for clarity.

Our main goal is to find the non-equilibrium spin polarization along the in-plane magnetic field. Indeed, all the quantum point contacts arranged along the channel are either the source or the drain of spins polarized along the magnetic field. In the absence of thermal effects we attribute therefore the non-local voltage to the excess spin polarization component along the applied magnetic field.

SO induced band mixing in a channel

Experimentally, [17] the BSR sets in at $E_Z \approx \hbar\omega$. We demonstrate that under this condition the SO interaction even if nominally weak, affects profoundly the spin dynamics. We start with the discussion of the effect of SO interaction on the electronic states in the channel. Let us denote the states in the absence of SO interaction as $|\psi^Z_{p,n,\sigma}\rangle$. These states by construction are eigenstates of the Hamiltonian, Eq. (1) with H_{SO} set to zero. The quantum numbers p, n and σ refer to the momentum along the channel, index of the subband of transversal quantization, and the spin index ($\sigma = \uparrow, \downarrow$) respectively. It follows from Eq. (1) that for $H_{SO} = 0$,

$$H|\psi^Z_{p,n,\uparrow(\downarrow)}\rangle = \left[\frac{p^2}{2m} \mp \frac{1}{2}E_Z + \varepsilon_n\right]|\psi^Z_{p,n,\uparrow(\downarrow)}\rangle\,. \tag{3}$$

When the condition $E_Z = \hbar\omega = \varepsilon_{n+1} - \varepsilon_n$ is satisfied the states $|\psi^Z_{p,n+1,\uparrow}\rangle$ and $|\psi^Z_{p,n,\downarrow}\rangle$ form a degenerate doublet, Fig. 2. Crucially, the SO interaction connecting these states strongly mixes them into a symmetric and antisymmetric combinations at the resonance, i.e. when the two states are degenerate.

As we are interested in low frequency and long wavelength phenomena we develop the low-energy description of the spin dynamics treating different pairs of degenerate doublets as independent. Such a description is valid as long as the typical energies of excitations we study are smaller than the inter-subband separation. The low-energy dynamics can then be formulated in terms of a pseudospin operating in the disconnected doubly degenerate subspaces of $|\psi^Z_{p,n+1,\uparrow}\rangle$ and $|\psi^Z_{p,n,\downarrow}\rangle$. We can therefore without loss of generality focus on a single pair of subbands $|\psi^Z_{p,n^*+1,\uparrow}\rangle$ and $|\psi^Z_{p,n^*,\downarrow}\rangle$ for a fixed n^* limited from above such that the bands we focus on are below the Fermi level.

We denote the Pauli matrices operating in the two-dimensional pdeudospin space as $\tau_{x,y,z}$. As we argued above we have to find the polarization along the applied magnetic field. Which is in turn given by the expectation value of the original σ_z Pauli matrix. Fortunately the two operators, σ_z and τ_z coincide when projected onto a pdeudospin subspace. Indeed,

$$\begin{bmatrix} \langle n^*+1,\uparrow|\sigma_z|n^*+1,\uparrow\rangle & \langle n^*+1,\uparrow|\sigma_z|n^*,\downarrow\rangle \\ \langle n^*,\downarrow|\sigma_z|n^*+1,\uparrow\rangle & \langle n^*,\downarrow|\sigma_z|n^*,\downarrow\rangle \end{bmatrix} = \begin{bmatrix} 1 & 0 \\ 0 & -1 \end{bmatrix} \equiv \tau_z \tag{4}$$

It follows that to study the dynamics of the real spin component σ_z it sufficient to focus on the dynamics of the pseudospin because within the pseudospin space we have $\sigma_z = \tau_z$ in view of Eq. (4).

The effective two by two Hamiltonian is the projection of the full Hamiltonian Eq. (1) into a pseudo-spin space spanned by $|\psi^Z_{p,n^*+1,\uparrow}\rangle$ and $|\psi^Z_{p,n^*,\downarrow}\rangle$. It can therefore be expressed in terms of the Pauli matrices operating in the pdeudo-spin space introduced above,

$$H_2 = \frac{p^2}{2m} + \frac{1}{2}(\varepsilon_{n^*} + \varepsilon_{n^*+1}) - \frac{1}{2}|g\mu_B|\mathbf{B}_{\mathrm{eff}} \cdot \boldsymbol{\tau}\,. \tag{5}$$

The effective magnetic field has the following non-zero components,

$$|g\mu_B|B_{\mathrm{eff},z} = E_Z - \hbar\omega\,, \qquad |g\mu_B|B_{\mathrm{eff},y} = \delta^{SO} = -2i\,\langle n^*+1,\uparrow|\alpha_- p_z \sigma_x|n^*,\downarrow\rangle\,. \tag{6}$$

The diagonal part of the *effective* magnetic field, a z-component accounts for the energy splitting between adjacent modes arising both from confinement ($\hbar\omega$) and from the Zeeman interaction with the actual external field (E_Z). The

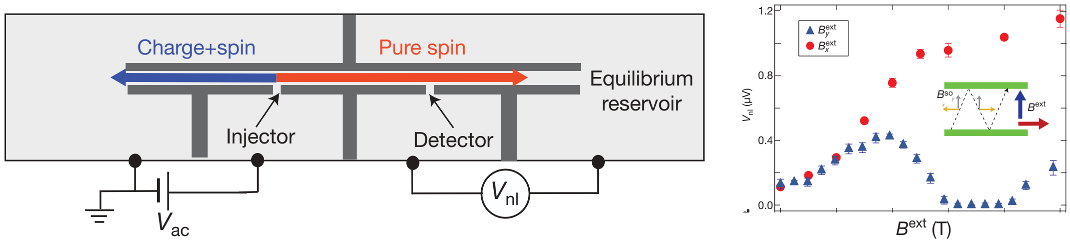

FIGURE 1. (left) Experimental setup schematics from Ref. [17]. The electric current is driven by the low frequency voltage source V_{ac}. As a result of the current drive the non-local voltage V_{nl} is induced at the right-most quantum point contact serving as a detector of non-equilibrium spin polarization. (right) Non-local voltage as a function of the in-plane magnetic field $B^{ext}(T)$ for the two orientations. The upper (lower) curve is obtained for the magnetic field along (perpendicular) orientation of the in-plane field.

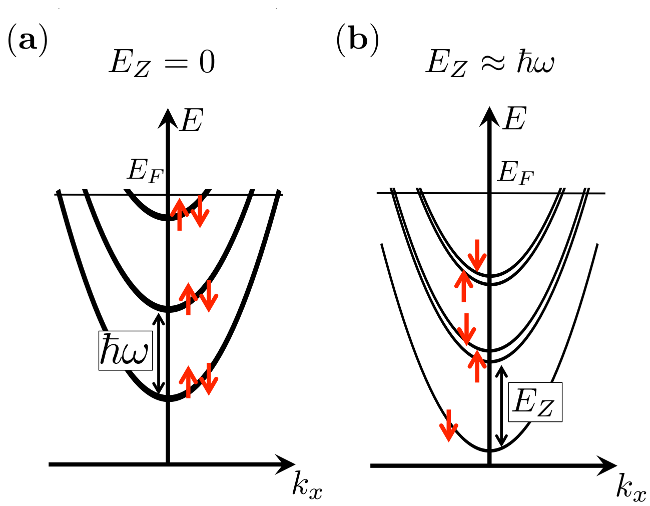

FIGURE 2. The band structure of the quasi-one-dimensional channel with k_x being the momentum along the channel, with the Fermi energy, E_F. The number of subbands of transversal quantization is reduced to three for clarity. In the experiment setup of Ref. [17] this number is close to few tens. (a) In the absence of the magnetic field, $E_Z = 0$ each state is doubly degenerate provided the SO energy scale is smaller than the typical inter-subband separation $\hbar\omega$. (b) Close to the BSR, the condition $E_Z \approx \hbar\omega$ is satisfied. As a result, the states $|n+1,\uparrow\rangle$ and $|n,\downarrow\rangle$ become nearly degenerate.

off-diagonal y-component of an effective field arises from SO matrix elements between states of differing spin and orbital quantum numbers (defined in the absence of SO).

Equation (6) shows why the magnetic filed has a strong effect on the spin polarization only when oriented perpendicularly to the channel, see Fig. 1 (right panel). The spin orientation $\uparrow$ ($\downarrow$) is defined relative to the direction of the magnetic field. Therefore, when the magnetic field is oriented along the channel, i.e. along x-axis, the effective magnetic field has only z-components and the effective Hamiltonian (5) is diagonal. It follows that the injected spins polarized along the magnetic field have no non-trivial spin dynamics. Therefore, the largest effect is achieved when the y component of the effective magnetic field is at maximum. This is achieved for the magnetic field oriented perpendicular to the channel in accordance with observation, see Fig. 1 (right panel).

The diagonalization of Eq. (5) is straightforward. It is useful to parametrize the effective field $\mathbf{B}_{\text{eff}}$ coupled to the pseudo-spin by the angle θ it forms with the *actual* magnetic field. We write

$$\mathbf{B}_{\text{eff}} = B_{\text{eff}}(0, \sin\theta, \cos\theta)\,. \tag{7}$$

The magnitude of the effective field, B_{eff} gives the subband splitting in the presence of the magnetic field and the SO interaction,

$$|g\mu_B|B_{\text{eff}} = \sqrt{(E_Z - \hbar\omega)^2 + |\delta^{SO}|^2}\,. \tag{8}$$

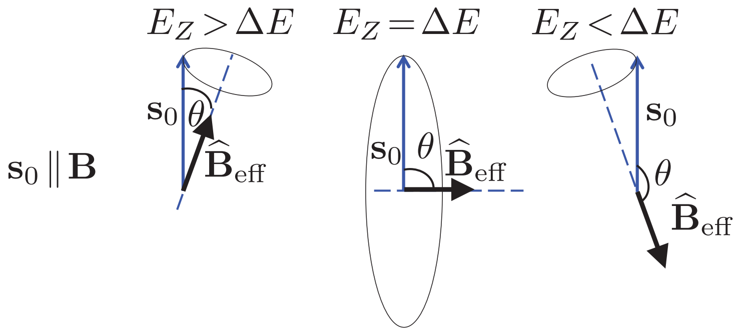

FIGURE 3. The injected spin polarization, $\boldsymbol{s}_0$, is directed along the external in-plane magnetic field $\mathbf{B} \parallel \hat{z}$. The inter-subband separation $\Delta E \equiv \hbar\omega$. The effective magnetic field $\mathbf{B}_{\text{eff}}$ defined by Eqs. (7), (8) and (9) determines the spin precession after injection. The z-component of $\mathbf{B}_{\text{eff}}$ vanishes at the resonance. In this case the spin dynamics is a pure precession with a frequency controlled by the SO coupling matrix element, $(g\mu_B/\hbar)\,|\mathbf{B}_{\text{eff}}| = (1/\hbar)\,|\langle n+1,\uparrow|\alpha p_z \sigma_x|n,\downarrow\rangle|$. Off resonance a finite component of injected spin ($\propto \cos\theta$) is conserved and is represented by an x-independent part in Eq. (18).

The angle θ parametrizing the matrix, Eq. (5), through the definition Eq. (7) reads

$$\cos\theta = \frac{E_Z - \hbar\omega}{\sqrt{(E_Z-\hbar\omega)^2 + |\delta^{SO}|^2}}\,, \qquad \sin\theta = \frac{\delta^{SO}}{\sqrt{(E_Z-\hbar\omega)^2 + |\delta^{SO}|^2}}\,. \tag{9}$$

The two SO split subbands are expressed in terms of the original bands in the absence of SO interaction as follows,

$$|\psi^{SO}_{k,+}\rangle = \alpha|\psi^Z_{k,n^*+1,\uparrow}\rangle + \beta|\psi^Z_{k,n^*,\downarrow}\rangle\,, \qquad |\psi^{SO}_{k,-}\rangle = \beta^*|\psi^Z_{k,n^*+1,\uparrow}\rangle - \alpha^*|\psi^Z_{k,n^*,\downarrow}\rangle\,, \tag{10}$$

where

$$\alpha = i\cos(\theta/2)\,, \quad \beta = -\sin(\theta/2)\,. \tag{11}$$

The energies of the eigenstates in Eq. (10) are

$$E^{SO}_{k,\pm} = \frac{\hbar^2 k^2}{2m} + \varepsilon^{SO}_{\pm}\,, \qquad \varepsilon^{SO}_{\pm} = \frac{1}{2}(\varepsilon_{n^*} + \varepsilon_{n^*+1}) \mp \frac{1}{2}\sqrt{(E_Z-\hbar\omega)^2 + |\delta^{SO}|^2}\,. \tag{12}$$

The band splitting

$$\varepsilon^{SO}_{-} - \varepsilon^{SO}_{+} = \sqrt{(E_Z-\hbar\omega)^2 + |\delta^{SO}|^2} \tag{13}$$

coincides with $|g\mu_B|B_{\text{eff}}$ defined by Eq. (8) as expected. Equations (10)-(12) specify the mixing effect of the SO coupling on the adjacent subbands shown schematically in Fig. 2(b).

Stationary spin polarization

We now compute the steady state spin polarization within the effective model specified by Eq. (5). To this end we assume that spins of a given polarization along z-axis are injected into a channel, and follow its dynamics relying on Eq. (5). The dc transport is determined by the states at the Fermi level. The Fermi wave vectors $k_\pm$ of the two subbands with the dispersion relations of Eq. (12) by definition satisfy $E_F = E^{SO}_{k_\pm,\pm}$, and are given by

$$k_\pm = \sqrt{\frac{2m}{\hbar^2}(E_F - \varepsilon^{SO}_{\pm})}\,. \tag{14}$$

Let the injector be placed at $x = x_s$ along the channel. The spinor wave function of the injected electron $|\Psi\rangle_{inj}$ is a superposition of the eigenstates given by Eq. (10). We can write this spinor as

$$|\Psi\rangle_{inj} = c_+|\psi^{SO}_{k_+,+}\rangle + c_-|\psi^{SO}_{k_-,-}\rangle\,, \tag{15}$$

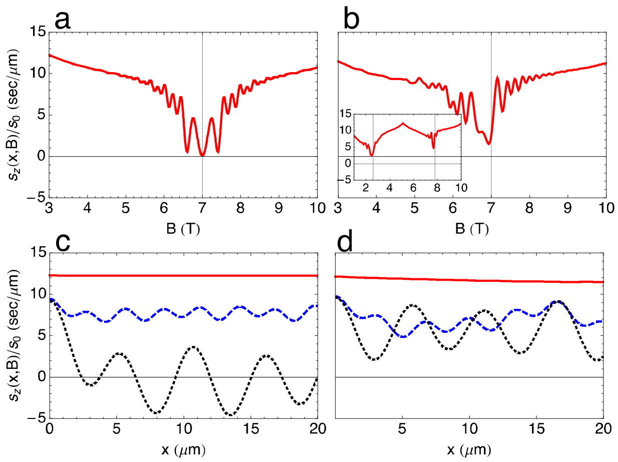

FIGURE 4. The stationary spin polarization s_z as a function of the magnetic field B for (a) parabolic and (b) square well lateral confinement. In all computations $\alpha_- = 2 \times 10^{-13}$ eV-m and the width of the injection aperture is 0.5μm. The effective mass is $m = 0.067m_e$ and the g factor is -0.44. The distance from the source, $x - x_s$, is 20μm in panels a and b. For square well confinement the width of the well, W, in panels (b) and (d) is 1.15μm The inset in panel (b) shows s vs B when $W = 3\mu$m and $x = 6.7\mu$m as in [17]. Except for the inset, the number of propagating modes (including spin) in all panels is 40. In the inset there are 105 propagating modes. Panels (c) and (d) show the dependence of the spin polarization on a distance from the source for the parabolic and square well lateral confinement respectively $B = 3$T (red,solid), $B = 6$T (blue,dashed), and $B = 7$T (black, dotted). The parameters used for parabolic confinement are $\mu = 3.65$ meV, $\hbar\omega = 0.1785$ meV, so that the magnetic field at the minimum is 7.0 T. For square well confinement $\mu = 1.86$ meV, whereas in the inset it is 1.765 meV. Parameters have been chosen to mimic those of Ref. [17].

where the Fermi wavevectors of the two SO split states are given by Eq. (14). If the injected spin is polarized along the z-direction the coefficients $c_\pm$ are, up to an overall phase factor, $c_+ = \alpha^*$ and $c_- = \beta$, where α and β are defined in Eqs. (9)-(11). The spin polarization $\tilde{s}_z(x,z) = \langle\Psi|\sigma_z|\Psi\rangle$ can be written using Eqs. (10) and (15) as follows:

$$\tilde{s}_z(x,z) = \left[|\alpha|^2 - |\beta|^2\right]\left[|\alpha|^2\phi_1^2(z) - |\beta|^2\phi_2^2(z)\right] + 2|\alpha|^2|\beta|^2\left[\phi_1^2(z) + \phi_2^2(z)\right]\cos\left[(k_+ - k_-)(x - x_s)\right]. \tag{16}$$

The spin polarization per unit length,

$$s_z(x) = \int dz\tilde{s}_z(x,z), \tag{17}$$

which is obtained from Eqs. (11) and (16), reduces to a simple expression that illustrates many of the key features of BSR:

$$s_z(x,B) = \cos^2\theta + \sin^2\theta\cos\left[(k_+ - k_-)(x - x_s)\right]. \tag{18}$$

We will refer to the part of $s_z(x,B)$ that does not oscillate with x as the *conserved* part of the spin density. The oscillation of the spin density is a result of the spatial beating of the two wave functions $|\psi^{SO}_{k_\pm,\pm}\rangle$, which propagate along the waveguide with phases $\exp[ik_\pm(x - x_s)]$. The equation (18) has a transparent meaning. The angle θ controls the spin dynamics as illustrated in Fig. 3. The component of the injected spin $\boldsymbol{s}_0$ along the effective field $\propto \cos\theta$ is conserved, while the component orthogonal to it $\propto \sin\theta$ undergoes the (pseudo)-spin precession. This difference in the spin dynamics is reflected in the different spatial modulations of the two components of the pseudo-spin in Eq. (18). We stress that as far as the diagonal component of the spin is concerned the spin and pseudo-spin are equivalent thanks to the identity (4).

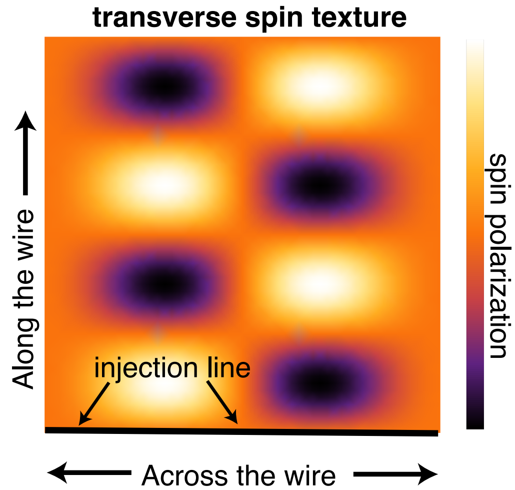

FIGURE 5. The spin texture $\tilde{s}_x(x,z)$ given by Eq. (18) at the resonance, $\cos\theta = 0$. and with only two subbands occupied. We therefore set $n^* = 1$ in Eq. (18). For the case of the square well confining potential we have $\phi_1(z) \propto \sin(\pi z/W)$ and $\phi_2(z) \propto \sin(2\pi z/W)$ where W is the width of the channel. The periodic modulation along the channel is due to the mismatch of the Fermi momenta, $k_+ \neq k_-$ of SO split subbands.

CONCLUSIONS

Physical interpretation of BSR. A key observation which follows from Eqs. (18) and (9) is that the non-oscillatory, a conserved part of the polarization $\propto \cos^2\theta$ vanishes at the resonance, $E_Z = \hbar\omega$. This by itself is not sufficient for the onset of the BSR which would imply vanishing of the spin polarization. We note however that the non-conserved part $\propto \sin^2\theta$ is subject to the disorder induced smearing. Even in purely ballistic situation the wave-length $l = 2\pi/(k_+ - k_-)$ of spin oscillations along the channel depends on the choice of the degenerate doublet labeled above by an integer n^*. This dependence is due to the variation in the matrix elements, $\langle n^*+1, \uparrow | \alpha_- p_z \sigma_x | n^*, \downarrow \rangle$ as well as the variation of the Fermi velocity with n^*. As the number of occupied subbands is relatively large ($\approx 30-40$) the contributions of the non-conserved spin polarizations from different n^* tend to interfere distructivly when added up. Another reason for suppression of the non-conserved polarization component is the finite size of the injector and detector which makes for a finite uncertainty in the phase in the second term of Eq. (18). The resulting spin polarization for realistic parameters are presented in Fig. 4 taken from Ref. [19].

Relationship between the spin and the pseudo-spin. The spin polarization along the magnetic field coincides with the pseudo-spin polarization along the same direction due to Eq. (4). This however cannot be said of other components of spin and pseudo-spin. Indeed since the spin-up and spin-down partners, $|\psi^Z_{k,n^*+1,\uparrow}\rangle$ and $\beta|\psi^Z_{k,n^*,\downarrow}\rangle$ have different orbital content, i.e. $n^* \neq n^*+1$ the *real* spin components $\sigma_{x,y}$ average out to zero once integrated over the channel's width, i.e.,

$$s_{x,y}(x) = \int dz \tilde{s}_{x,y}(x,z) = 0, \tag{19}$$

where $\tilde{s}_{x,y}(x,z) = \langle \Psi | \sigma_{x,y} \Psi \rangle$. The result (19) is due to the orthogonality of transversal modes of quantization labeled by *different* indices n^* and n^*+1. This result means that the spin polarization perpendicular to the external magnetic field oscillate in space with periodicity determined by the energy scales $E_Z \approx \hbar\omega$. These oscillations are outside the range of applicability of the effective model as given by Eq. (5). It should be contrasted with the precession of the pseudo-spin, $\boldsymbol{\tau}$ which is identical to the standard spin precession in the presence of Zeeman field as evidenced by Eq. (5).

Effect of the disorder. Effects of the disorder were investigated in the work [19]. With the main conclusion that the ballistic spin resonance survives the disorder with the shape of the non-local voltage dependence being affected although not the position of the dip as compared to the ballistic case presented in Fig. 4. See also [23] for alternative approach.

Spin texture at the resonance. The second important observation refers to the presence of the spin texture in the channel. Although $s_{x,y}(x) = 0$ according to (19), the local spin density $\tilde{s}_{x,y}(x,z)$ is in general non-zero. The resulting spin texture for the model of the two subbands labeled by n^* and n^*+1 considered above is

$$\tilde{s}_x(x,z,B) \propto \sin[(k_+ - k_-)(x - x_s)]\phi_{n^*}(z)\phi_{n^*+1}(z)\,, \tag{20}$$

which is obtained similarly to Eq. (16). The spin texture is illustrated for the single pair of occupied subbands in Fig. 5.

ACKNOWLEDGMENTS

We thank J.A. Folk and A.M. Finkel'stein for useful discussions. M.K. acknowledges the support of the University of Iowa. M.E.F. was supported in part by C-SPIN, one of six centers of STARnet, a Semiconductor Research Corporation program, sponsored by MARCO and DARPA.

REFERENCES

1. S. A. Wolf, D. D. Awschalom, R. A. Buhrman, J. M. Daughton, S. von Molnár, M. L. Roukes, A. Y. Chtchelkanova, and D. M. Treger, *Science* **294**, 1488–1495 (2001).
2. D. D. Awschalom, and M. E. Flatté, *Nature Physics* **3**, 153–159 (2007).
3. S. Datta, and B. Das, **56**, 665–667 (1990).
4. J. Schliemann, J. C. Egues, and D. Loss, **90**, 146801 (2003).
5. K. Hall, and M. E. Flatté, **88**, 162503 (2006).
6. S. Heedt, C. Morgan, K. Weis, D. E. Bürgler, R. Calarco, H. Hardtdegen, D. Grützmacher, and T. Schäpers, *Nano Letters* **12**, 4437–4443 (2012).
7. A. Bournel, P. Dollfus, P. Bruno, and P. Hesto, *Eur. Phys. J. AP* **4**, 1–4 (1998).
8. A. A. Kiselev, and K. W. Kim, *Phys. Rev. B* **61**, 13115–13120 (2000).
9. T. P. Pareek, and P. Bruno, *Phys. Rev. B* **65**, 241305 (2002).
10. A. G. Mal'shukov, and K. A. Chao, *Phys. Rev. B* **61**, R2413–R2416 (2000).
11. Y. V. Pershin, *Phys. Rev. B* **71**, 155317 (2005).
12. P. Schwab, M. Dzierzawa, C. Gorini, and R. Raimondi, *Phys. Rev. B* **74**, 155316 (2006).
13. S. Lüscher, S. M. Frolov, and J. A. Folk, *Phys. Rev. B* **82**, 115304 (2010).
14. A. W. Holleitner, V. Sih, R. C. Myers, A. C. Gossard, and D. D. Awschalom, *Phys. Rev. Lett.* **97**, 036805 (2006).
15. V. A. Froltsov, *Phys. Rev. B* **64**, 045311 (2001).
16. F. E. Meijer, A. F. Morpurgo, T. M. Klapwijk, T. Koga, and J. Nitta, *Phys. Rev. B* **70**, 201307 (2004).
17. S. M. Frolov, S. Lüscher, W. Yu, Y. Ren, J. A. Folk, and W. Wegscheider, *Nature* **458**, 868–871 (2009).
18. S. M. Frolov, A. Venkatesan, W. Yu, J. A. Folk, and W. Wegscheider, *Phys. Rev. Lett.* **102**, 116802 (2009).
19. D. H. Berman, M. Khodas, and M. E. Flatté, *Phys. Rev. X* **4**, 011048 (2014).
20. E. I. Rashba, *Soviet Physics Solid State* **2**, 1109–1122 (1960).
21. Y. A. Bychkov, and E. I. Rashba, *J. Phys. C* **17**, 6039–6045 (1984).
22. G. Dresselhaus, *Phys. Rev.* **100**, 580–586 (1955).
23. M. O. Hachiya, G. Usaj, and J. C. Egues, *Phys. Rev. B* **89**, 125310 (2014).